9-1-2020

Tensile and superelastic behaviors of Ti-35Nb-2Ta-3Zr with gradient structure

Liqiang Wang

Yingchen Wang

Wei Huang

Jia Liu

Yujin Tang

See next page for additional authors

10.1016/j.matdes.2020.108961

Wang, L., Wang, Y., Huang, W., Liu, J., Tang, Y., Zhang, L., ... & Lu, W. (2020). Tensile and superelastic behaviors of Ti-35Nb-2Ta-3Zr with gradient structure. Materials & Design, 194, article 108961. https://doi.org/10.1016/j.matdes.2020.108961

Materials and Design 194 (2020) 108961

Contents lists available at ScienceDirect

Materials and Design

journal homepage: www.elsevier.com/locate/matdes

Tensile and superelastic behaviors of Ti-35Nb-2Ta-3Zr with gradient structure

Liqiang Wang [a,b], Yingchen Wang [b], Wei Huang [b], Jia Liu [a,*], Yujin Tang [a], Ling Zhang [c,*], Yuanfei Fu [d], Lai-Chang Zhang [e,*], Weijie Lu [b]

[a] Affiliated Hospital of Youjiang Medical University for Nationalities, Baise, Guangxi 533000, China
[b] State Key Laboratory of Metal Matrix Composites, School of Material Science and Engineering, Shanghai Jiao Tong University, No. 800 Dongchuan Road, Shanghai 200240, China
[c] Electron Microscopy Center of Chongqing University, International Joint Laboratory for Light Alloys (MOE), College of Materials Science and Engineering, Chongqing University, Chongqing 400045, China
[d] Ninth People's Hospital, School of Medicine, Shanghai Jiao Tong University, Shanghai 200011, China
[e] School of Engineering, Edith Cowan University, 270 Joondalup Drive, Joondalup, Perth, WA 6027, Australia

HIGHLIGHTS

- Ti35Nb2Ta3Zr processed by double-faced friction stir processing obtained roughly 2 times higher yield strength.
- Superelasticity showed different tendency after friction stir process.
- Higher strength in stir zone and better ductility in heat affected zone were confirmed by in situ microcompression tests.

GRAPHICAL ABSTRACT

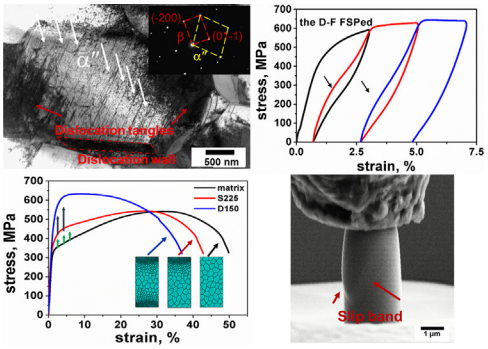

ARTICLE INFO

Article history:
Received 4 February 2020
Received in revised form 15 June 2020
Accepted 7 July 2020
Available online 12 July 2020

Keywords:
β titanium alloy
Surface modification
Friction stir processing
Gradient structure

ABSTRACT

We investigated the tensile and superelastic behaviors of Ti-35Nb-2Ta-3Zr processed by double-faced friction stir processing that results in a roughly 2 times higher yield strength with an elongation of 37%. The friction stir processed specimens exhibited different superelasticity as loading cycle increased. To assess the strength and deformation of gradient structure, in situ micro compression tests were conducted on stir zone and heat affected zone, revealing higher strength in stir zone and better ductility in heat affected zone. The combination of stir zone and heat affected zone could increase the strength and maintain the ductility of the specimen simultaneously.

1. Introduction

β titanium alloy has been used extensively in biomedical applications due to their relatively low Young's modulus, good biocompatibility, outstanding corrosion and wear resistance [1–6]. Nevertheless, low service strength of β titanium alloy limited its application in the

* Corresponding authors.
E-mail addresses: liujia0111@live.cn (J. Liu), zhangling2014@cqu.edu.cn (L. Zhang), lczhangimr@gmail.com (L.-C. Zhang).

https://doi.org/10.1016/j.matdes.2020.108961

field of load-bearing implants. For enhancement of the mechanical properties, constructing nanostructure processed by severe plastic deformation technologies has been reported previously [7–10]. However, the significant increase of strength brings about tremendous reduction in ductility and increment of modulus. Single structure can not satisfy internal and external biological environment simultaneously. Therefore, gradient structure with nanostructure surface has attracted lots of attention [11–13]. Lu et al. found gradient boundary migration process accompanied a simultaneously continuous grain growth, resulting a 10 times higher yield strength without a reduction of ductility [14]. Wei et al. produced a gradient nanotwinned structural TWIP steel and found the hierarchical nanotwins contributed to the increase of the yielding strength and interactions of twin-twin accompanying with dislocation-twin maintained the ductility [15]. Bahrami et al. synthesized Ti-Ta coatings by confocal dual magnetron co-sputtering, which achieved high elasticity and better adhesion to a soft metallic substrate [16]. In addition, plenty of applications were also discussed. Yasaman et al. designed and 3D-printed gradient-structured scaffolds, which improved integration of scaffolds with native tissue [17]. Nan et al. fabricated the structural/compositional gradient nanofibrous scaffolds, which had the potential to induce interfacial tissue regeneration [18]. Sana et al. summarized existing cell-free approaches and confirmed sustained value of gradient structural materials [19]. Though many researchers reported the preparation and application of gradient structural materials, very few studies on the gradient structural β titanium alloy have been reported.

Recently, many researchers have tried to use friction stir processing technology (FSP), a novel solid-state surface modification technique, to modify the materials' surface to improve mechanical properties [20–24]. Four regions, including stir zone (SZ), transition zone (TZ), heat affected zone (HAZ) and matrix, can be observed in the FSPed materials from upper surface [25,26]. However, much effort has already been taken to investigate the SZ of the FSPed materials and few reports investigate the gradient structure of β titanium alloy after FSP [27–30]. Therefore, we tried to introduce FSP to process the Ti-35Nb-2Ta-3Zr layers in order to achieve a gradient structure of β titanium alloy and

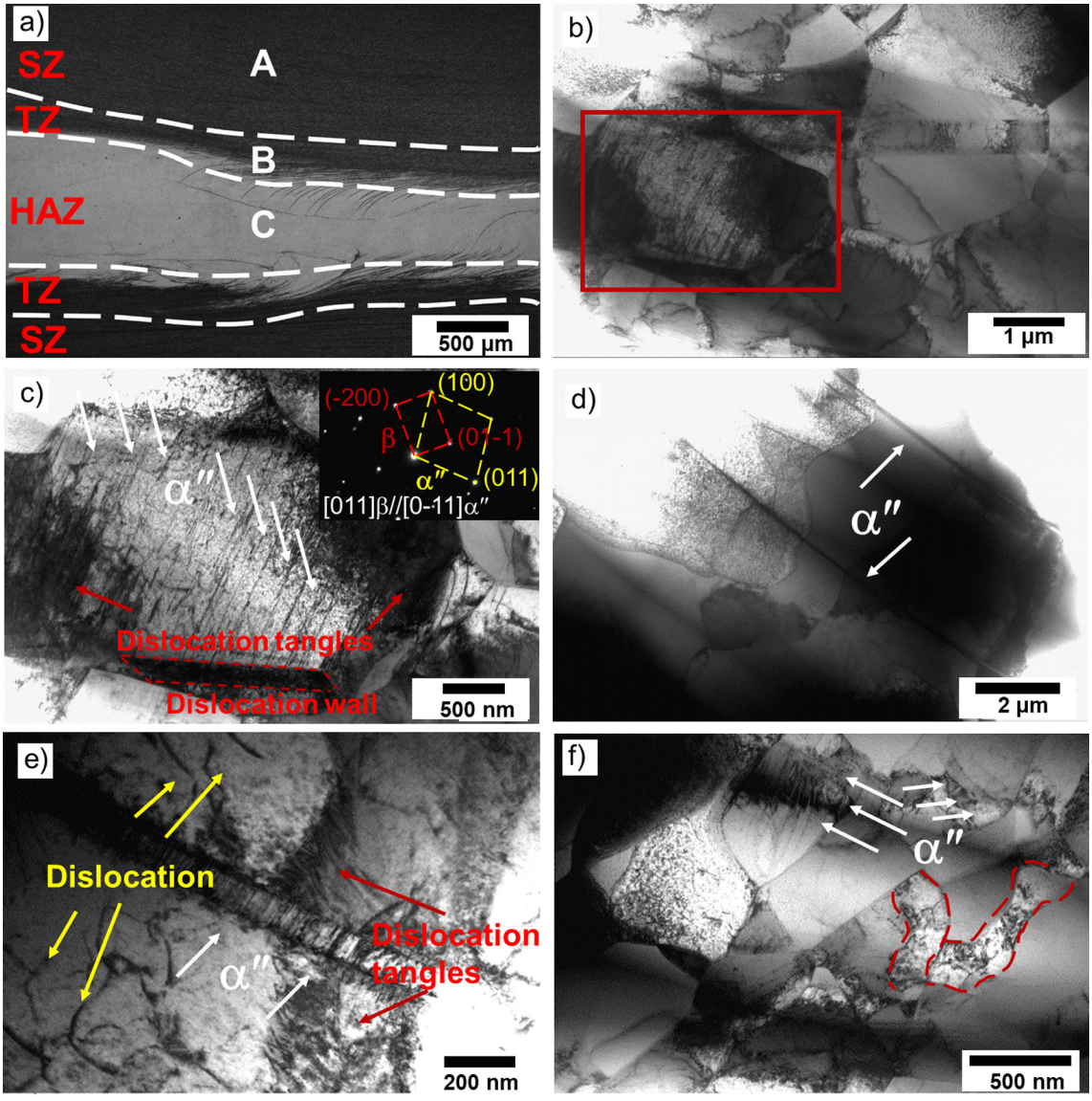

Fig. 1. Microstructure of the double-faced FSPed specimen: (a) optical image, and TEM images of (b) recrystallized grains in region A in stir zone, (c) needle-shaped martensite phase inside the recrystallized grain (the red box in (b)), (d) martensite phase in the transition zone, (e) martensite phase in the transition zone at a higher magnification, (f) dislocation tangles, martensite phase and the elongated grains in the heat affected zone.

investigate the contribution of the gradient structure to mechanical properties. In our work, we would construct a gradient structure from surface to core through processing both the upper and lower surfaces of the layer by FSP. We investigated the contribution of the gradient structure and the deformation mechanism by the tensile tests and the micropillar compression.

2. Materials and methods

The Ti-35Nb-2Ta-3Zr plate with a thickness of 5 mm was processed via FSP using W-Re alloy tool in an argon atmosphere. We used two methods to build different gradient structural materials. The first was processing the upper surface with probe diameter of 12 mm and probe plunge depth of 1.7 mm at rotation speed of 225 rpm and travel speed of 50 mm/min. The second was processing both the upper and lower surfaces with probe diameter of 12 mm and probe plunge depth of 0 mm at rotation speed of 150 rpm and travel speed of 50 mm/min.

The microstructures were characterized by transmission electron microscopy (TEM) in a JEM 2100 microscope operated at 200 kV. TEM specimens were cut from designated depth (0.2 mm, 0.7 mm, 2.0 mm) and ion thinned to a thickness of 100 nm. Tensile specimens with gauge section of 10 × 6 × 3.5 mm (L × W × H) were cut along the process path. During friction stir process, thickness of specimens was reduced by thermo-mechanical treatment. Final thickness of samples for tensile tests was therefore 3.5 mm. Room temperature tension tests were performed at a strain rate of 1×10^{-3} s^{-1}, using a Zwick Z100/SN3A universal testing machine. The cyclic tensile tests were carried out at strains of 3%, 5% and 7%, respectively. The specimens after the tensile tests for micrographs were cut, ground, polished and etched with a volume ratio 1:3:10 of HF:HNO_3:H_2O, and characterized in a Nova FEI 400 field emission scanning electron microscope (SEM). The micropillar was fabricated by focusing ion beam (FIB) using SciosDualBeam with the current range of 15–0.1 nA, gradually reduced to match the micropillar dimensional accuracy of the layer-by-layer

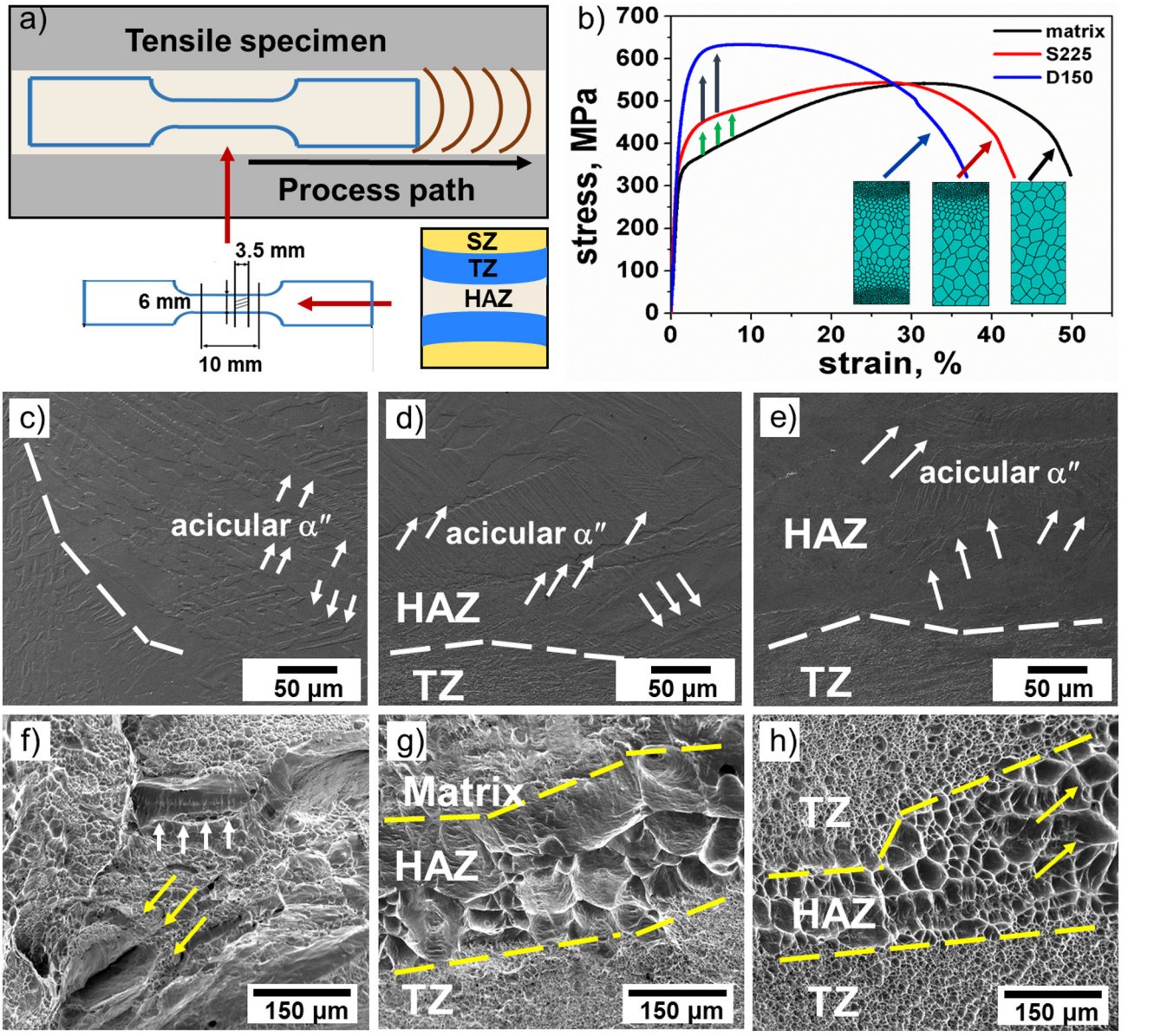

Fig. 2. (a) Schematic illustration of the position, shape and size for the tensile specimen; (b) Stress- strain curves obtained by tensile tests; SEM images of microstructures along the tensile direction after the tensile tests of (c) the matrix, (d) the single-faced FSPed specimen and (e) the double-faced FSPed specimen; SEM images of the fracture surface of (f) the matrix, (g) the single-faced FSPed specimen and (h) the double-faced FSPed specimen.

peeling. Micropillars with diameter of 2 μm and height of 6 μm were obtained. Micropillar compression is performed under displacement controlled mode in a Zeiss Auriga SEM-FIB equipped with a Hysitron PI88 system, with a constant compression rate at 5 nm/s during compression.

3. Results and discussions

Fig. 1 (a) shows the optical microstructure in transversal cross-section of the double-faced (D-F) FSPed specimen. A gradient structure with several distinct regions can be consecutively observed from the upper surface to the lower surface, including sitr zone (SZ), transition zone (TZ) and heat affected zone (HAZ), respectively. Grains in as-cast beta titanium alloy obtain a large size, which has been widely studied [31]. After FS process, grains are refined to varying degrees. Similar to former research, grains size shows a decreasing trend [29] from internal to the surface. Fig. 1 (b)–(c) show the TEM images of stir zone (i.e, region A in Fig. 1 (a)). From Fig. 1 (b), there is no distinct anisotropy and almost equiaxed grains are uniformly distributed with an average grain size less than 2 μm, consistent with the occurrence of dynamic recrystallization in references [25]. In Fig. 1 (c) (the red box in Fig. 1 (b)), massive parallel needle-shape α″ martensite with more than 2 μm in length and less than 50 nm in width occur inside the recrystallized grain. Dislocation tangles and dislocation walls can be found around the grain boundaries, as indicated by the yellow arrows. In transition zone, much coarser martensitic laths can be found across the grains and a mass of dislocations distribute in the grain internal and around the interface, as shown in Fig. 1 (d) and (e). The area in transition zone undergoes the plastic deformation suffered by shearing force and stress from stir zone with shorter excursion time and lower temperature. Therefore, the stress-induced α″ martensite nucleates and grows quickly in transition zone, resulting in longer and wider stress-induced α″ martensite. As seen from heat affected zone in Fig. 1 (f), a pile of dislocations gather around the grain boundaries. In addition, plate-shaped α″ martensite inside the grains and elongated grains along processing direction are observed, as illustrated in Fig. 1 (f). During friction stir processing, heat affected zone with high depth undergoes high forces, which will such induce the martensitic transformation. According to Lee's research, martensite growth can be blocked by high-angle grain boundary, instead of low-angle grain boundary [32]. Grains in HAZ achieve a larger size than grains in SZ, density of grain boundary in HAZ is relatively low. With fewer obstacles from grain boundary, martensite in HAZ grows coarser than that in SZ.

Fig. 2 (a) shows schematic illustration of the position, shape and size for the tensile specimen. Fig. 2 (b) depicts the curves of the tensile tests at the strain rate of $1 \times 10^{-3}\ s^{-1}$. Compared with the matrix, the single-faced (S-F) FSPed sample has a light increase of the yield strength from ~300 MPa to ~350 MPa. However, the double-faced (D-F) FSPed sample has a significant increase in yield strength from ~300 MPa to ~550 MPa and an increase in ultimate tensile strength from ~540 MPa to ~630 MPa, with an elongation of 37% simultaneously. As shown in Fig. 2 (b), the curves of both the matrix and the S-F FSPed have a relatively flat plateau, indicating stress-induced martensite transformation and the initiation of slip deformation of α″ martensite. Fig. 2 (c)–(e) illustrates the typical microstructures of the matrix, the S-F FSPed and the D-F FSPed along the tensile direction after the tensile tests. Seeing from Fig. 2 (c), indicating the matrix feature after the tensile test, bunchy stress-induced martensite occurred inside the grain and around the boundaries, changing from acicular martensite to butterfly shaped martensite. With increasing deformation during the tensile test, the combination of shear of slip bands and interaction of plate-shaped martensite refines the plate-shaped martensite, indicated by white arrows in Fig. 2 (c). In Fig. 2 (d) and (e), we find the distinct regions of TZ and HAZ for the S-F FPSed and the D-F FSPed specimens after tensile tests. Drape-shaped martensite in TZ and plate-shaped martensite and thin acicular martensite in HAZ are investigated. Furthermore, the acicular martensite in HAZ of the D-F FSPed are less than that of S-F FSPed, as depicted by white arrows in Fig. 2 (d) and (e). In addition, Wang et al. investigated the dynamic recrystallization mechanism of stir zone and transition zone of FSPed β titanim alloy and obtained the nanoscale grains through three-pass FSP [29]. In our work, we construct a gradient structure with submicroscale and microscale grains. During loading period, substantial grain growth could occur and accommodate the large plastic strains in gradient structure [14]. According to Hall-Petch relationship, coarser grains have smaller yield strength. Plastic deformation occurs first in coarse grains, then propagates into refined grains as load increases. In this orderly deformation process, strain localization is suppressed by releasing intergranular stress, hence excellent ductility is

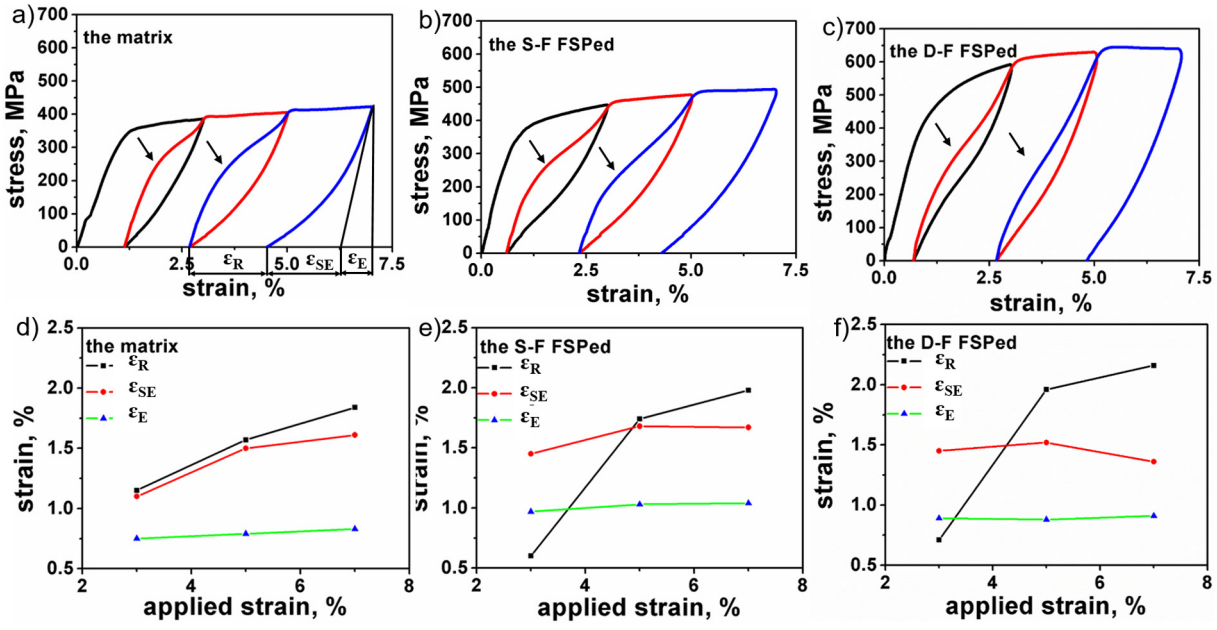

Fig. 3. Stress-strain curves obtained by cyclic loading-unloading tests for (a) the matrix, (b) the single-faced FSPed specimen and (c) the double-faced FSPed specimen; ε_R, ε_{SE} and ε_E extacted from the stress-strain curves at strain of 3%, 5% and 7% of (d) the matrix, (e) the single-faced FSPed specimen and (f) the double-faced FSPed specimen.

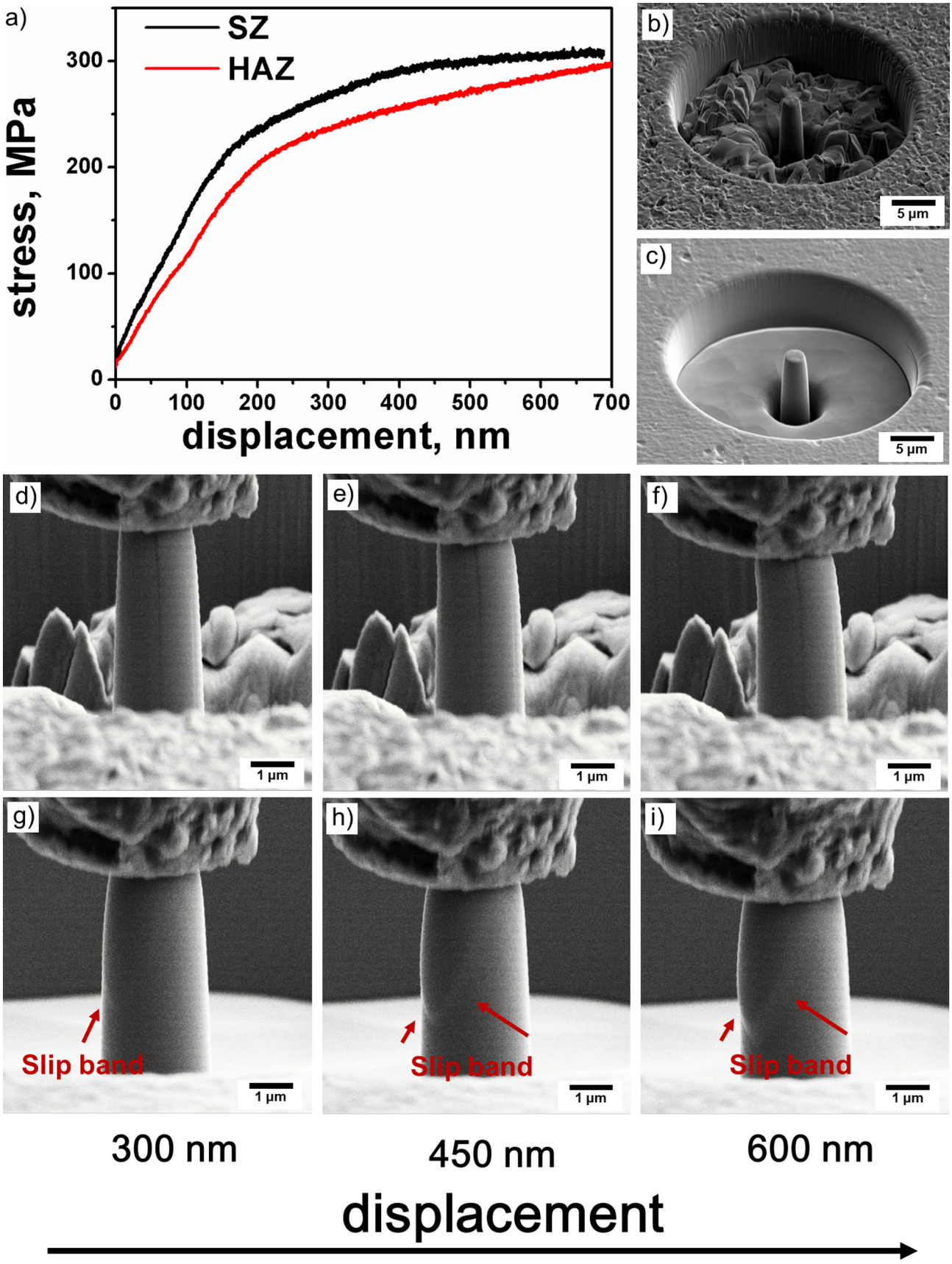

Fig. 4. (a) Stress-displacement curves of SZ and HAZ from micropillar compression tests of the D-F FSPed specimen; Representative morphology of the fabricated micropillars of the D- F FSPed specimen in (b) SZ and (c) HAZ; SEM snapshots of pillars in SZ compressed to the displacements in (d) 300 nm, (e) 450 nm, (f) 600 nm; SEM snapshots of pillars in HAZ compressed to the displacements in (g) 300 nm, (h) 450 nm, (i) 600 nm.

ensured [11]. Meanwhile, microscale and submicroscale grains contribute to considerable fine grain strengthening. Therefore, the gradient structure starting from micro-submicro grains achieves both high strength and excellent ductility.

Fig. 2 (f)–(h) display the SEM micrographs of the fracture surface of the matrix, the S-F FSPed and the D-F FSPed tensile tested specimens, respectively. The fracture morphologies reveal ductile fracture in overall specimens. The matrix tolerates a good deal of elongation before the breakage with deep simples. As seen in Fig. 2 (g) and (h), dimples in HAZ are obviously lager than that in TZ, contributing to plasticity of the D-F FSPed tensile tested specimen. Besides, dimples in HAZ of S-F FSPed specimen are even larger than that in HAZ of D-F FSPed specimen, which corresponds to higher elongation of S-F FSPed alloy. Two friction stir processes lead to more severe deformation, hence D-F FSPed specimen has higher residual stress. Residual stress facilitates the fracture, confirmed by Li et al. [33], which can explain the difference of ductility between S-F and D-F FSPed specimens.

Fig. 3 (a), (b) and (c) display stress-strain curves of cyclic loading-unloading tensile tests for the matrix, the S-F FSPed and the D-F FSPed specimens, respectively. Residual strain (ε_R), superelastic strain (ε_{SE}) and pure elastic strain (ε_E) of corresponding specimens are shown in Fig. 3 (d), (e) and (f). It has been studied that deformation-induced twin martensite could contribute much to superelasticity [29,34]. According to former research, obstacles to extended dislocations and appropriate stacking fault energy accelerate martensite nucleation [35,36]. Pre-deformed specimens have more dislocations, hence twin martensite is easier to be induced during loading. Consequently, more superelastic strain could recover during unloading. However, the growth of martensite is hindered by dislocation as well. As a result, superelastic strain rises sluggishly or even declines, which is shown in Fig. 3 (e) and (f). In contrast, matrix is not pre-deformed. Lower dislocation density provides less driving force to induce martensite, hence ε_{SE} after the first cycle is relatively small. Meanwhile, dislocation hindering has less influence on growth of stress-induced martensite, which means martensite-inducing mechanism is the dominant factor during subsequent loading process. Therefore, ε_{SE} of matrix could increase continuously with the number of cycles, as shown in Fig. 3 (d).

The stress-displacement curves of micropillar in SZ and HAZ of the D-F FPSed specimen are plotted in Fig. 4 (a). The slope of the stress-displacement in SZ is obviously higher than that in HAZ in elastic stage. The strength of the micropillar in SZ is higher than that in HAZ. The typical morphology of the fabricated SZ and HAZ micropillars is shown in Fig. 4 (b) and (c). Fig. 4 (d)–(k) shows the SEM microphology of the micropillar in SZ and HAZ with the displacements in 300 nm, 450 nm, and 600 nm,respectively. With the increase of the displacement, no significant shape change is observed in SZ micropillar. Due to the largest plastic deformation and axial stress during processing, in the SZ, the grains were finest (Fig. s1) and the dislocation intense was the highest. Based on the Hall-Patch relationship, the yield strength of SZ was markedly improved. According to former research, ω phase could nucleate from β matrix during severe plastic deformation and transforms into α" martensite [29]. It is reasonable to believe the existence of ω phase. These particles also trap movement of dislocations and contribute to high strength. In contrast, obvious slip bands develop on the surface of the micropillar in HAZ during the whole compression test without forming a sharp section, which promotes the plasticity of the the D-F FSPed specimen. Compared with nanoscale and submicroscale grains, the coaser grains have better plasticity. The combination of SZ and HAZ constructs a gradient structure, improving the yield strength and maintaining the plasticity of the material.

4. Conclusion

In summary, we obtain a gradient structure by using friction stir processing to process the upper surface and lower surface of the Ti-35Nb-2Ta-3Zr layers. Different shapes of stress-induced martensite appear from stir zone to heat affected zone in the double-faced FSPed specimen due to the different plastic deformation feature and heat input. Through the tensile tests and the cyclic tensile tests, the double-faced FSPed specimen shows excellent yield strength and superelasticity. Furthermore, we investigated the deformation behavior of SZ and HAZ separately by the micropillar compression tests. Stir zone has higher strength, and heat affected zone has better plasticity, since dislocation slip contributes to much more plastic deformation. This research produces a new insigh to improve β titanium alloy mechanical properties.

Declaration of Competing Interest

We declare that we have no financial and personal relationships with other people or organizations that can inappropriately influence our work, there is no professional or other personal interest of any nature or kind in any product, service and/or company that could be construed as influencing the position presented in, or the review of, the manuscript entitled.

Acknowledgement

This research was funded by the National Natural Science Foundation of China (No. 31971246, No.51674167, No.51831011). High-level Innovation team and Outstanding Scholars Program of Colleges and University in Guangxi: Innovative team of basic and Clinical Comprehensive Research on Bone and Joint Degenerative Diseases.

Appendix A. Supplementary data

Supplementary data to this article can be found online at https://doi.org/10.1016/j.matdes.2020.108961.

References

[1] L.M. Elias, S.G. Schneider, S. Schneider, et al., Microstructural and mechanical characterization of biomedical Ti–Nb–Zr(–Ta) alloys, Mater. Sci. Eng. A. 432 (2006) 108–112.
[2] Y. Guo, D. Chen, M. Cheng, et al., The bone tissue compatibility of a new Ti35Nb2Ta3Zr alloy with a low Young's modulus, Int. J. Mol. Med. 31 (2013) 689–697.
[3] N. Hafeez, S. Liu, E. Lu, et al., Mechanical behavior and phase transformation of β-type Ti-35Nb-2Ta-3Zr alloy fabricated by 3D-printing, J. Alloy. Compd. 790 (2019) 117–126.
[4] S. Liu, J. Liu, L. Wang, et al., Superelastic behavior of in-situ eutectic-reaction manufactured high strength 3D porous NiTi-Nb scaffold, Scr. Mater. 181 (2020) 121–126.
[5] C.D. Rabadia, Y.J. Liu, L. Wang, et al., Laves phase precipitation in Ti-Zr-Fe-Cr alloys with high strength and large plasticity, Mater. Des. 154 (2018) 228–238.
[6] C.D. Rabadia, Y.J. Liu, L.Y. Chen, et al., Deformation and strength characteristics of laves phases in titanium alloys, Mater. Des. 179 (2019) 107891.
[7] R.Z. Valiev, T.G. Langdon, Principles of equal-channel angular pressing as a processing tool for grain refinement, Prog. Mater. Sci. 51 (2006) 881–981.
[8] A.P. Zhilyaev, T.G. Langdon, Using high-pressure torsion for metal processing: fundamentals and applications, Prog. Mater. Sci. 53 (2008) 893–979.
[9] L. Wang, W. Lu, J. Qin, et al., Influence of cold deformation on martensite transformation and mechanical properties of Ti–Nb–Ta–Zr alloy, J. Alloy. Compd. 469 (2009) 512–518.
[10] K. Wu, H. Chang, E. Maawad, et al., Microstructure and mechanical properties of the Mg/Al laminated composite fabricated by accumulative roll bonding (ARB), Mater. Sci. Eng. A. 527 (2010) 3073–3078.
[11] K. Lu, Making strong nanomaterials ductile with gradients, Science. 345 (2014) 1455–1456.
[12] X.L. Wu, P. Jiang, L. Chen, et al., Synergetic strengthening by gradient structure, Mater. Res. Lett. 2 (2014) 185–191.
[13] J. Ding, Q. Li, J. Li, et al., Mechanical behavior of structurally gradient nickel alloy, Acta. Mater. 149 (2018) 57–67.
[14] T.H. Fang, W.L. Li, N.R. Tao, et al., Revealing extraordinary intrinsic tensile plasticity in gradient nano-grained copper, Science. 331 (2011) 1587–1590.
[15] Y. Wei, Y. Li, L. Zhu, et al., Evading the strength–ductility trade-off dilemma in steel through gradient hierarchical nanotwins, Nat. Comm. 5 (2014) 3580.
[16] A. Bahrami, J.P. Álvarez, O.D. Rivera, et al., Compositional and Tribo-mechanical characterization of Ti-Ta coatings prepared by confocal dual magnetron Co-sputtering, Adv. Eng. Mater. (2017) 1700687.

[17] Y. Zamani, G. Amoabediny, J. Mohammadi, et al., 3D-printed poly(ε-caprolactone) scaffold with gradient mechanical properties according to force distribution in the mandible for mandibular bone tissue engineering, J. Mech. Behav. Biomed. 104 (2020) 103638.
[18] N. Jiang, J. He, W. Zhang, et al., Directed differentiation of BMSCs on structural/compositional gradient nanofibrous scaffolds for ligament-bone osteointegration, Mater. Sci. Eng. C 110 (2020) 110711.
[19] S. Ansari, S. Khorshidi, A. Karkhaneh, Engineering of gradient osteochondral tissue: from nature to lab, Acta. Biomater. 87 (2019) 41–54.
[20] L.C. Zhang, L.Y. Chen, L.Q. Wang, Surface modification of titanium and titanium alloys: technologies, developments, and future interests, Adv. Eng. Mater. 22 (2020) 1901258.
[21] W. Wang, P. Han, P. Peng, et al., Friction stir processing of magnesium alloys: a review, Acta. Metall. Sin. (English Letters) (2019) 43–57.
[22] Z. Ding, C. Zhang, L. Xie, et al., Effects of friction stir processing on the phase transformation and microstructure of TiO2-compounded Ti-6Al-4V alloy, Metall. Mater. Tran. A. 47 (2016) 5675–5679.
[23] C. Zhu, Y. Lv, C. Qian, et al., Proliferation and osteogenic differentiation of rat BMSCs on a novel Ti/SiC metal matrix nanocomposite modified by friction stir processing, Sci. Rep. 6 (2016) 38875.
[24] C. Zhang, Z. Ding, L. Xie, et al., Electrochemical and in vitro behavior of the nanosized composites of Ti-6Al-4V and TiO2 fabricated by friction stir process, Appl. Surf. Sci. 423 (2017) 331–339.
[25] L. Wang, J. Qu, L. Chen, et al., Investigation of deformation mechanisms in beta-type Ti-35Nb-2Ta-3Zr alloy via FSP leading to surface strengthening. Metall. Mater. Tran. A. 46 (2015) 4813–4818.
[26] Z. Ding, Q. Fan, L. Wang, A review on friction stir processing of titanium alloy: characterization, method, microstructure, properties, Metall. Mater. Tran. B. 50 (2019) 2134–2162.
[27] H. Gu, Z. Ding, Z. Yang, et al., Microstructure evolution and electrochemical properties of TiO2/Ti-35Nb-2Ta-3Zr micro/nano-composites fabricated by friction stir processing, Mater. Des. 169 (2019) 107680.
[28] R. Ran, W. Liu, L. Wang, et al., alpha" martensite and amorphous phase transformation mechanism in TiNbTaZr alloy incorporated with TiO2 particles during friction stir processing, Metall. Mater. Tran. A. 49 (2018) 1986–1991.
[29] L. Wang, L. Xie, Y. Lv, et al., Microstructure evolution and superelastic behavior in Ti-35Nb-2Ta-3Zr alloy processed by friction stir processing, Acta. Mater. 131 (2017) 499–510.
[30] A. Zafari, X.S. Wei, W. Xu, et al., Formation of nanocrystalline β structure in metastable beta Ti alloy during high pressure torsion: the role played by stress induced martensitic transformation, Acta. Mater. 97 (2015) 146–155.
[31] Y. Guo, K. Georgarakis, Y. Yokoyama, et al., On the mechanical properties of TiNb based alloys, J. Alloys Compd. 571 (2013) 25–30.
[32] S. Lee, C. Park, J. Hong, et al., Development of sub-grained α+β Ti alloy with high yield strength showing twinning- and transformation-induced plasticity, J. Alloys Compd. 813 (2020) 152102.
[33] Y. Li, X. Ren, J. He, et al., Effect of thermal residual stresses on ductile-to-brittle transition of a bi-material specimen by using the CAFE method, Eur. J. Mech. A-Solid. 80 (2020) 103889.
[34] N. Hafeez, J. Liu, L. Wang, et al., Superelastic response of low-modulus porous beta-type Ti-35Nb-2Ta-3Zr alloy fabricated by laser powder bed fusion, Addit. Manuf. 34 (2020) 101264.
[35] L. Wang, L. Xie, L. Zhang, et al., Microstructure evolution and superelasticity of layer-like NiTiNb porous metal prepared by eutectic reaction, Acta. Mater. 143 (2018) 214–226.
[36] L. Wang, C. Wang, L. Zhang, et al., Phase transformation and deformation behavior of NiTi-Nb eutectic joined NiTi wires, Sci. Rep. 6 (2016) 23905.